Hydrogen embrittlement I. Analysis of hydrogen-enhanced localized plasticity: Effect of hydrogen on the velocity of screw dislocations in α-Fe

Ivaylo H. Katzarov,[1,2] Dimitar L. Pashov,[1] and Anthony T. Paxton[1]
[1]*Department of Physics, King's College London, Strand, London WC2R 2LS, United Kingdom*
[2]*Bulgarian Academy of Science, Institute of Metal Science, 67, Shipchenski prohod Str., 1574 Sofia, Bulgaria*
(Received 24 April 2017; revised manuscript received 14 June 2017; published 8 August 2017)

We demonstrate a kinetic Monte Carlo simulation tool, based on published data using first-principles quantum mechanics, applied to answer the question: under which conditions of stress, temperature, and nominal hydrogen concentration does the presence of hydrogen in iron increase or decrease the screw dislocation velocity? Furthermore, we examine the conditions under which hydrogen-induced shear localization is likely to occur. Our simulations yield quantitative data on dislocation velocity and the ranges of hydrogen concentration within which a large gradient of velocity as a function of concentration is expected to be observed and thereby contribute to a self-perpetuating localization of plasticity—a phenomenon that has been linked to hydrogen-induced fracture and fatigue failure in ultrahigh strength steel. We predict the effect of hydrogen in generating debris made up of edge dipoles trailing in the wake of gliding screw dislocations and their role in pinning. We also simulate the competing effects of softening by enhanced kink-pair generation and hardening by solute pinning. Our simulations act as a bridge between first-principles quantum mechanics and discrete dislocation dynamics, and at the same time offer the prospect of a fully physics-based dislocation dynamics method.

DOI: 10.1103/PhysRevMaterials.1.033602

I. INTRODUCTION

A. Hydrogen-enhanced local plasticity

Hydrogen has well known and devastating effects on the toughness of high strength steel. It is widely accepted that a detailed theory of hydrogen embrittlement is still lacking, while at the same time a number of putative mechanisms has been put forward. Among these are the familiar "hydrogen-enhanced decohesion" (HEDE) the subject of the second in this sequence of two papers [1], and the "hydrogen-enhanced localized plasticity" (HELP), which is the subject of the present paper. There are two fundamentally difficult questions that arise when considering these two processes [2]: (i) if the effect of internally supplied hydrogen is to enhance cracking, how is this possible in the case that the crack speed is greater than the speed of hydrogen diffusion to the crack tip in order to feed the decohesion? (ii) If the effect of hydrogen is to enhance plasticity, how can this lead to a propensity for fracture, since plasticity is generally regarded as increasing toughness through crack tip blunting? While at the first glance HEDE and HELP seem unconnected, they are in fact intimately so. Ultimately there must be decohesion for there to be cracking; on the other hand, the fracture is always accompanied by large amounts of plasticity and indeed it is thought that hydrogen has the effect of *localizing* plasticity, which may lead to failure by fracture at a lower stress than in the absence of hydrogen. It is generally thought that the effect of hydrogen is to facilitate dislocation glide by increasing the dislocation velocity and by reducing, or screening, the elastic interactions between dislocations. Here, we make explicit calculations of the velocity of a screw dislocation in α-Fe as a function of applied shear stress, temperature, and bulk hydrogen concentration. These central results of this paper are shown in Figs. 12–14 below. We are able to identify those regimes in which the dislocation velocity is either enhanced or reduced by hydrogen. In the second paper in the series [1], we consider just the idealized case of a crystal of α-Fe separating across a (111) crystal plane under the influence of a bulk concentration of hydrogen. We are able to calculate the crack opening as a function of stress, temperature, and bulk hydrogen concentration and to find the reduction in fracture stress. The method we use will be extended in future work to look at decohesion across other crystal planes, grain boundaries, and at dislocation pile ups. What is very evident from our work is that since the bulk hydrogen concentration is typically only in the parts per million range due to its very limited solubility in α-Fe, it is the *tensile stress* at the decohering planes, or indeed at the crack tip, that is attracting the hydrogen into sufficient quantity to cause damage. This is, therefore, a time limited process since the rate of decohesion must be matched by the rate of diffusion. These effects are included in our model [1]. What links these two papers together is indeed their separateness: it is vital to able to factor the two processes of HELP and HEDE, and in particular to evaluate the reduction of the cohesive strength only as a result of stress driven hydrogen diffusion and its segregation to the cohesive zone.

The HELP mechanism is based on observations that in a range of temperatures and strain rates, the presence of hydrogen in solid solution decreases the barriers to dislocation motion, thereby increasing their mobility and allows highly localized deformation. A third possible mechanism for hydrogen embrittlement is the "hydrogen-enhanced stress-induced vacancy" (HESIV) process [3]. We focus in this paper on HELP, but as a consequence of our simulations we are able to identify the origin of the stress-induced vacancies called upon by HESIV.

The possibility of enhanced ductile processes resulting from hydrogen in metals was first put forward by Beachem [4]. Strong evidence for failure by hydrogen-enhanced local plasticity has been obtained by macroscopic flow stress measurements, fractographic evidence, *in situ* TEM studies, measurements of dislocation motion, and theoretical treatments [5–8]. This evidence of enhanced plasticity, resulting in localized plastic failure, suggests that hydrogen promotes

shear decohesion along slip planes in contrast to the usual sense of segregation embrittlement by *tensile* decohesion arising from a reduced work of fracture. The physics that lies behind enhanced dislocation motion due to hydrogen is not yet established. A comprehensive understanding of the HELP mechanism requires a more detailed reckoning than can be provided by phenomenology; where at the continuum level, supportive arguments for hydrogen-induced slip localization have been supplemented by Birnbaum *et al.* [9]. These include theoretical findings related to dislocation mobility, shear localization, and elastic shielding of the interaction of dislocations with stress centers.

Some progress can be made by incorporating information from more accurate atomistic calculations at smaller length scales into continuum models. Fully discrete simulations using empirical potentials also have been used to model the interaction of hydrogen with dislocations but the predictive power of these studies is to a great extent limited by the reliability of the interatomic potential [10]. On the other hand, first-principles calculations are mostly limited to studies of bulk phases, point defects, simple grain boundaries, and dislocation core structures [11,12].

Kirchheim views hydrogen embrittlement based on enhanced localized plasticity in the light of a defactant concept [13–15], describing solute-defect interaction in a thermodynamic framework. According to this concept, solute atoms segregated to defects, such as vacancies, dislocations, jogs and kinks in dislocation lines, lower the defect formation energy. In particular, within the defactant concept solute atoms affect both kink formation and kink motion on screw dislocations [16].

A possible cause of hydrogen embrittlement by the HELP mechanism is the softening of materials by hydrogen solute atoms arising from increased screw dislocation mobility and reduced flow stress when hydrogen atoms are introduced into bcc metals. If a concentration of hydrogen atoms induces local slip, the increase of local strain and dislocation density (and hence density of trap sites for hydrogen) leads to further concentrations of hydrogen atoms through the defactant effect, followed by plastic instability and ductile fracture through a self-perpetuating reinforcement of the process.

Plasticity in bcc metals is mainly mediated by the thermal activation of kink pairs on screw dislocation lines. Since the mobility of dislocations in bcc metals is mainly determined by that of the screw component, investigation of the interaction between a screw dislocation and a hydrogen atom plays a key role in understanding the HELP mechanism.

The structure of this paper is as follows. In Sec. I B, we outline the present work and place it in context. Section II describes the kinetic Monte Carlo approach that we use, with Sec. II A explaining its application to the screw dislocation in α-Fe, Sec. II B the generation of stable kink pairs as the principal agent of the glide of the screw dislocation, and Sec. II B the migration of the kinks. Section III is our results and discussion section: Sec. III A gives details of the model and Sec. III B describes the microstructures that we observe as a result of the kMC simulations. In Sec. III C, we make connection to the HESIV mechanism. Section III D presents our results of calculated transients in the dislocation velocity and Sec. III E gives the results of the dislocation velocity in the steady state, including the effects of temperature, applied stress, and nominal hydrogen concentration in solid solution. We conclude in Sec. IV.

B. Outline of the present work

We base the present work upon some rather seminal recent papers [11,17,18] employing the density functional theory (DFT) to calculate (i) the interaction energy between a hydrogen interstitial and a screw dislocation, (ii) the kink-pair formation energy, and (iii) the kink migration energy; the latter two as functions of hydrogen concentration. These data were used to fit parameters to a line tension model [11,17]. This model was applied to bcc α-Fe to determine the kink-pair formation enthalpy at different applied stresses. The effect of hydrogen on the mobility of a screw dislocation in α-Fe was investigated [18] and it was found that hydrogen lowers the Peierls barrier when a hydrogen atom is trapped ahead of the screw dislocation on the slip plane. A hydrogen atom trapped behind the dislocation line can slow or stop the kink motion and decrease the dislocation mobility. The softening effect of hydrogen atoms by promoting kink nucleation and the hardening effect by impeding the kink movement were both evaluated [18].

DFT results show that the $\frac{1}{2}[111]$ screw dislocation core in α-Fe is nondegenerate and spreads onto the three $\{\bar{1}10\}$ planes [11,12]. This nonplanar core structure significantly affects screw dislocation mobility. Kink pairs can nucleate on either of the three $\{\bar{1}10\}$ planes, while kink migration is constrained to its own glide plane. The collision of kinks moving on these different planes results in the generation of jogs, on which cusps are formed through the accumulation of kinks. The short segment of a jog lies in a different glide plane from the parent line and its configuration is such that often glide of the parent line requires climb of the jog segment. For these reasons jogs are almost always impediments to dislocation glide and are often sessile segments that pin the dislocation locally.

The present work aims at exploring the mobility of $\frac{1}{2}[111]$ screw dislocations in α-Fe through simulation of the specific mechanisms of motion of an individual dislocation. Determination of the dislocation mobility from simulations requires tracking the dynamics of individual dislocations over relatively long time scales. Given the inherently small time scales of first-principles calculations and atomic level simulations such as molecular dynamics (MD), such simulations are rarely possible today. In order to overcome this limitation, we use a kinetic Monte Carlo (kMC) simulation of $\frac{1}{2}[111]$ screw dislocations and track their glide in order to obtain a realistic description of the dynamics of a dislocation line over long time scales [19]. The advantage of this approach is that it replaces arbitrary assumptions about the nature of dislocation mobility with input based upon microscopic understanding and explicit quantum mechanical calculations [18].

The kMC method is computationally less expensive than MD because the interatomic interactions are not computed directly as the simulation proceeds. Instead, kMC uses precomputed transition rates along the minimal energy paths between the metastable sites, thereby allowing employment of precise electronic structure methods. Our kMC model also allows dislocations to cross slip onto secondary glide planes [20,21]. Thus motion of screw dislocations becomes fully three dimensional.

II. KINETIC MONTE CARLO

A. kMC model of a screw dislocation in bcc metal

A kinetic Monte Carlo simulation method for modeling screw dislocation motion in bcc metals was proposed by Cai *et al.* [20]. Due to the high Peierls barrier [22,23], the motion of ordinary screw dislocations in α-Fe is believed to be controlled by nucleation, migration and annihilation of kinks. When the stress on a dislocation is lower than its Peierls stress, the dislocation line stays at rest in a given lattice position, interrupted by the thermally assisted process of kink-pair nucleation. The separation of kinks under the influence of stress and thermal activation results in translation of the entire dislocation line to the next Peierls valley. In this way, the overall dislocation movement is the cumulative effect of a large number of individual kink events.

The nonplanar core of $\frac{1}{2}[111]$ screw dislocations spreads symmetrically on three cross-slip $\{\bar{1}10\}$ planes and their glide is not confined to a single glide plane. In fact, each screw dislocation segment can nucleate kink pairs on either of the three $\{\bar{1}10\}$ planes—a mechanism by which screw dislocations change their glide planes. The kMC model does not consider any details of the core structure. It focuses on dislocation motion on length and time scales far greater than those of atomistic simulations. The key idea of the kMC approach is to treat dislocation motion as a stochastic sequence of discrete rare events whose mechanisms and rates are computed within the framework of transition state theory. Dislocations are represented as interconnected small straight segments in an elastic continuum. Local stresses resulting from applied loading and internal stresses are computed on each of those segments.

We model the screw dislocation as a piece wise straight line stretched along the [111] direction. While the dislocation has, on average, a screw orientation, it consists of screw (S) and edge (E) dislocation segments such that kinks on the screw dislocation are perfect edge segments. The approximation of finite width kinks by edge segments with zero width is appropriate when the kink width is smaller than the distance between two kinks in a kink pair. Both the line tension model [17] and molecular dynamics simulations of $\frac{1}{2}[111]$ screw dislocations in bcc Fe [11] show that the kink width $w_k \approx 10b$ and kinks in a stable kink pair are separated by distances $w_{kp} \approx 30b$. We choose

$$a = b = \tfrac{1}{2}a_0[111] \tag{1}$$

for the length of S segments, where b is the Burgers vector of the screw dislocation and $a_0 = 2.87$ Å is the lattice constant of α-Fe. The three-dimensional space is discretized in the form of a grid having a and h (the unit kink height) as grid spacings in the screw and edge directions, respectively. This is a hexagonal lattice, with axial parameter a in the [111] direction, and basal parameter h.

Kink pairs are allowed to nucleate in any of the three $\{\bar{1}10\}$ glide planes intersecting the [111] direction. Once nucleated, a kink (E segment) can move in its glide plane along the dislocation line until it recombines with another kink with the opposite sign, collides with a kink moving on a different plane or reaches the end of the line. During kMC simulations, the dislocation moves under the action of applied shear stress through kink-pair nucleation, migration, collision and recombination. This model does not allow for climb of the edge segments.

The kinetics of dislocation motion is completely specified by the matrix of transition rates. Transition state theory expresses the rates of kink-pair nucleation and kink migration events in terms of their respective energy barriers. The following form of transition rate matrix provides a physically consistent description of the energetics and thermally activated formation of a double kink:

$$J_{kp}(\sigma_{eff}) = f_{kp}\ \exp\left(-\frac{\Delta E_{kp}(\sigma_{eff})}{k_B T}\right).$$

$\Delta E_{kp}(\sigma_{eff})$ is the stress dependent activation energy of kink-pair formation, k_B is the Boltzmann constant and f_{kp} is the pre-exponential "frequency" factor. The local resolved stress

$$\sigma_{eff} = \sigma_{app} + \sigma_{self} + \sigma_{solute}$$

comprises the applied stress, the self-stress field and stress field associated with the solute atoms. The self-stress is the stress exerted on a dislocation segment by all other dislocation segments and can be calculated from the gradient of the self energy due to virtual displacements [24]. Details of the calculation of the self stress may be found elsewhere [19]. The total energy is computed using the non singular continuum theory of dislocations [24]. The major advantage of this theory is that it contains no singularities. The divergence arises from the inadequacy of linear elastic theory to deal with severe lattice distortions near the core of the dislocation. Thus the treatment is restricted to the matter outside a cylinder of radius r_c where linear theory should apply. The nonsingular expression for dislocation energy depends on the choice of the cut off parameter r_c. The shape and the kink-pair energy have been determined by Itakura *et al.* [17] via the line tension model parameterized to DFT calculations. The calculated kink-pair energy is 0.69 eV [17]. In the present work, we approximate the kink-pair shape predicted by the line tension model and MD simulations [11,17] by two sharp kinks separated by distances $w_{kp} = 30b$. We determine the cut off parameter r_c by comparing the energies of kinks separated by distances w_{kp}, predicted by non singular continuum theory, with the corresponding data obtained by the line tension model. The value of the cut off parameter is $r_c = 0.48b$.

We use our kMC model to calculate the $\frac{1}{2}[111]$ screw dislocation mobility in α-Fe at fixed applied stresses of 50, 100, and 200 MPa; temperatures of 150, 300, and 400 K and various hydrogen concentrations in the range zero to 300 appm (atomic parts per million). The total length of the S segments are $L = 1000b = 0.245$ μm, while each E segment length is $h = 2.31$ Å. This length of the dislocation line in our simulations is close to the typical measured length of screw dislocations in α-Fe [25] and permits sufficient freedom for self pinning of the dislocation due to the formation of jogs and superjogs.

B. Stable kink-pair nucleation

At finite temperature the long straight screw dislocation in bcc metals does not lie quiescent in its Peierls valley. Instead, it suffers spontaneous thermally activated nucleations of kink

pairs. Following the nucleation of an elementary kink pair, the kinks are most frequently so close together that the elastic attraction between them is strong enough to result in immediate annihilation. String method simulations of kink nucleation and migration [17] and our tight binding nudged elastic band (NEB) simulations of the same process show that the width of an embrionic kink pair is about $10b$ [26]. A *stable* kink pair is one that has sufficient distance between the kinks, which we take to be about $30b$, that elastic attraction is small enough to allow the kink pair to survive and its halves to separate under the local stresses they encounter. The formation of a stable kink pair is a result of numerous acts of kink-pair nucleation, annihilation, and increasing distance between kinks under the action of the applied shear stress. We do not consider all these processes explicitly in our simulations. Instead we use experimental results for nucleation rates of stable kink pairs.

The kMC model employs the rates of kink-pair nucleation events, expressed in terms of their respective energy barriers. DFT calculations have been used in Ref. [17] to identify the minimal energy path of a screw dislocation core between two adjacent Peierls valleys and to evaluate the Peierls barrier ΔE_{kp}. The interaction energy between a screw dislocation and hydrogen atoms has been calculated for various hydrogen positions and dislocation configurations [18]. A line tension model of a dislocation [18] incorporating these first-principles calculations has been used to predict the kink-pair activation energy with hydrogen, $\Delta E_{\mathrm{kp,H}}$, and without hydrogen, ΔE_{kp}, for various shear stresses applied in a $\{\bar{1}10\}$ plane in the [111] direction. The effect of hydrogen on kink-pair nucleation enthalpy is that a hydrogen atom lowers the Peierls barrier when it is trapped in the core ahead of the dislocation line on the slip plane. Our NEB simulations of kink-pair nucleation and growth show that a hydrogen atom reduces the kink-pair nucleation energy when it is trapped ahead of kink-pair nucleus with width about $10b$ [26]. The reduction of kink nucleation enthalpy by hydrogen, ΔE_{H}, was estimated to be about 110 meV for all the applied stress cases [18].

A general tendency in bcc metals is a discrepancy between the atomistic scale calculations of kink-pair nucleation enthalpy ΔE_{kp} and experimental measurements [22]. This has been attributed to several origins, such as pile up effects and neglect of zero-point energy in the energetics of the proton [17]. For this reason, in our kMC model, we use experimentally determined kink-pair activation energies [18,22]. To account for the effect of a hydrogen atom trapped in the core ahead of the dislocation line, we reduce the nucleation enthalpy by $\Delta E_{\mathrm{H}} = 110$ meV, assumed independent of the local stress [18]. We then have

$$\Delta E_{\mathrm{kp,H}} = \Delta E_{\mathrm{kp}} - \Delta E_{\mathrm{H}}.$$

In the present work, we determine the frequency prefactor f_{kp} by comparing the velocity of the pure screw segment in pure α-Fe calculated from kMC with the experimentally estimated velocity [25]. The prefactor comes out as $f_{\mathrm{kp}} = 2.31 \times 10^{9}\ \mathrm{s}^{-1}$.

If a hydrogen atom is trapped just behind the dislocation line, its relative position to the dislocation core changes after formation of a kink pair ahead of it, and its solution energy increases by $E_{\mathrm{t}} = 179$ meV [18]. During the kink-pair nucleation process, N hydrogen atoms trapped behind a dislocation segment with width $w_{\mathrm{kp}} = 30b$ exert a local effective stress [24]:

$$\sigma_{\mathrm{solute}} = \frac{N E_{\mathrm{t}}}{2 w_{\mathrm{kp}} b h}.$$

The local stress field σ_{solute} is one of the components of the resolved local stress σ_{eff}, which determines the local activation energy $\Delta E_{\mathrm{kp}}(\sigma_{\mathrm{eff}})$ of kink-pair formation.

TABLE I. Calculated dislocation velocities, v_0, in pure iron, at the temperatures and stresses used in the present work. These data are the quantities v_0 that appear on the ordinates of Figs. 9–14. These are the results of simulations of a single $\frac{1}{2}[111]$ screw dislocation of length 245 nm (noting that in the absence of pinning the dislocation velocity is proportional to its length). At 300 K, the velocities calculated by the kMC model for a local shear stress $\sigma = 33$ MPa are in good agreement with the measurements of Caillard [25].

T (K)	σ_{app} (MPa)	v_0 (nm s^{-1})
150	50	4.13×10^{-9}
	100	4.69×10^{-5}
	200	6.10×10^{3}
300	50	10.65
	100	1.10×10^{3}
	200	1.25×10^{7}
400	50	2.46×10^{3}
	100	7.68×10^{4}
	200	8.38×10^{7}

C. Kink migration

A kink, once formed, can migrate along the dislocation line. The rate of migration of the kinks depends on the magnitude of the activation energy for kink motion. If this secondary Peierls barrier is very large the kink migration is thermally activated. MD simulations show that typical applied stresses far exceed the secondary Peierls barrier which leads to a high mobility of nucleated kinks [27]. The low secondary Peierls stress mean that kink migration along the screw dislocation is not thermally activated but is limited by phonon drag. Therefore, in our kMC model, the thermally activated migration events specified by the transition rates are replaced by continuous movement of the kinks with velocity proportional to the stress of the dislocation line calculated at the current instant in time [20,28]. The kink velocity v_{k} is proportional to the driving force experienced by the kink,

$$v_{\mathrm{k}} = \sigma_{\mathrm{g}} \frac{b}{B}, \tag{2}$$

where σ_{g} is the glide component of the resolved shear stress, b the Burgers vector, and B the phonon drag coefficient. In the present work we use the temperature dependent value of the drag coefficient for kink motion $B = (2.7 + 0.008T) \times 10^{-5}$ Pa s, determined by MD simulations [27].

If a hydrogen atom is trapped just behind the dislocation line, and a kink sweeps past the hydrogen atom, its relative position to the dislocation core changes, and its solution energy increases by $E_{\mathrm{t}} = 179$ meV. (See Ref. [18], Fig. 6 and Table I.) The kink trapping barrier E_{t} is reduced as the applied shear stress σ_{eff} increases. The values of $E_{\mathrm{t}}(\sigma)$ for various applied

shear stress have been calculated using the line tension model [18], and it is these that we take for our simulations.

Kinks require thermal activation to overcome the trapping energy barrier associated with hydrogen atoms behind the core. The velocity with which a kink bypasses a solute along its path is [24,28]

$$v_{\mathrm{k}} = \frac{\sigma b h}{k_{\mathrm{B}} T} a^2 P_{\mathrm{H}}, \tag{3}$$

where

$$P_{\mathrm{H}} = f_{\mathrm{k}} \exp\left(-\frac{E_{\mathrm{t}}(\sigma)}{k_{\mathrm{B}} T}\right)$$

is the rate at which a kink passes a hydrogen atom situated in the Peierls valley just behind the dislocation line. The attempt frequency f_{k} is of the order of the Debye frequency (1.34×10^{13} s^{-1} for iron) and a is the jump distance (1). However, not all kinks will move forward after passing the hydrogen atom behind the dislocation line. Some of them will return to the initial lower energy state. In this way, we assert that

$$J_{\mathrm{k}}^{+} = f_{\mathrm{k}} \exp\left(-\frac{\Delta E - \sigma a^2 h}{k_{\mathrm{B}} T}\right)$$

and

$$J_{\mathrm{k}}^{-} = f_{\mathrm{k}} \exp\left(\frac{E_{\mathrm{t}} - \sigma a^2 h}{k_{\mathrm{B}} T}\right)$$

are the rates of forward and backward jumps from the new kink position [24]. The change in energy ΔE when the kink moves forward is calculated using non singular elastic theory. The probability that the kink will move forward upon passing the hydrogen atom behind the dislocation line before moving back to the lower energy state is

$$P^{+} = \frac{J_{\mathrm{k}}^{+}}{J_{\mathrm{k}}^{+} + J_{\mathrm{k}}^{-}}.$$

The rate P_{H}^{+} at which a kink passes a hydrogen atom behind the dislocation line and continues its movement forward can be obtained from the rate at which the kink bypasses a hydrogen atom, P_{H}, and the corresponding survival probability P^{+},

$$P_{\mathrm{H}}^{+} = P_{\mathrm{H}}\, P^{+}.$$

Inserting P_{H}^{+} into (3), we obtain the velocity with which a kink bypasses a hydrogen atom before continuing its forward movement:

$$v_{\mathrm{k}} = \frac{\sigma b h}{k_{\mathrm{B}} T} a^2 P_{\mathrm{H}}^{+}. \tag{4}$$

We describe the motion of kinks using (2) at all times other than when the kink encounters a hydrogen atom, in which case we employ (4).

As a final ingredient to the model we need to specify the bulk hydrogen concentration, C_{H}. For a chosen hydrogen loading, normally given in atomic parts per million (appm) we can find the equilibrium hydrogen concentration C_d at a binding site with a binding energy E_{b} around the dislocation core using the McLean isotherm [18],

$$C_d = \frac{\frac{1}{3} C_{\mathrm{H}} \exp\left(\frac{E_{\mathrm{b}}}{k_{\mathrm{B}} T}\right)}{1 + \frac{1}{3} C_{\mathrm{H}} \exp\left(\frac{E_{\mathrm{b}}}{k_{\mathrm{B}} T}\right)} \tag{5}$$

III. RESULTS AND DISCUSSION

A. Model details

The typical value of hydrogen concentration in the bulk in industrial environments and in charged samples in experiments at room temperature are correspondingly 0.1 appm and 10 appm. The equilibrium hydrogen concentration C_d at the strongest hydrogen binding sites with binding energy 256 meV calculated from McLean's equation for bulk concentrations of 10 appm at 300 K is about 0.05. At room temperature, the typical hydrogen concentration in the bulk is large enough to concentrate less than one hydrogen atom ahead of kink-pair nucleus with width $10b$. In this work, we study the effect of hydrogen on dislocation mobility when the average number of hydrogen atoms trapped ahead of an embrionic kink pair is no more than one. In this case, the occupancy of the strongest hydrogen binding sites does not exceed $C_{\max} = 0.1$. The equilibrium hydrogen concentration $C_{\max}$ corresponds to bulk concentrations of about 0.001, 20, and 200 appm for temperatures of 150, 300, and 400 K.

Since the prefactor f_{H} of the hydrogen diffusion rate in bulk,

$$J_{\mathrm{H}} = f_{\mathrm{H}} \exp\left(-\frac{E_{\mathrm{H}}}{k_{\mathrm{B}} T}\right),$$

is orders of magnitude higher than f_{kp}, the condition $\Delta E_{\mathrm{kp,H}} > E_{\mathrm{H}}$ sets an upper critical shear stress $\sigma_c \approx 250$ MPa, above which hydrogen diffusion cannot catch up with dislocation motion [18]. For applied shear stresses in the range $\sigma_{\mathrm{app}} =$ 50–200 MPa, used in the present simulations, the time scale of hydrogen diffusion is much shorter than that of dislocation migration. This means that below σ_c, the hydrogen diffusion is fast compared to screw dislocation motion, and the hydrogen density at the core trap sites is approximated well by C_d (5). Using the calculated equilibrium concentrations (5), we randomly generate the positions of the hydrogen atoms trapped in the binding sites around the dislocation core. Since the time scale of hydrogen diffusion is much longer than that of kink migration and orders of magnitude shorter than the time scale of kink-pair nucleation, we generate new positions of hydrogen atoms trapped in the core before nucleation of a new kink pair. In this, we maintain approximate local equilibrium of the hydrogen in bulk and defect trap sites.

Several different shear stress orientations of the maximum resolved shear stress (MRSS) plane have been tested in our kMC simulations: from symmetrical double slip conditions to symmetrical and nonsymmetrical slip on one primary and two secondary $\{\bar{1}10\}$ planes. In the special case of symmetrical double slip, kink-pair nucleation is equally probable on two planes. Hence we may expect a growing probability for collision of kinks nucleated in two distinct slip planes. In the case of symmetrical triple slip conditions, the MRSS plane is parallel to the primary glide plane making the resolved shear stress on the primary glide plane much larger than that in the secondary planes. Since kink pairs mostly nucleate on the

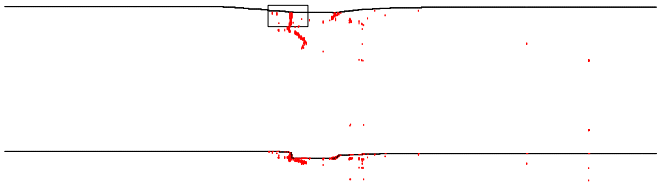

FIG. 1. Snapshot of a moving $\frac{1}{2}[111]$ screw dislocation (black line) in pure α-Fe projected onto $(\bar{1}10)$ and $(11\bar{2})$ planes as upper and lower lines, respectively. The red lines indicate debris left behind due to the creation of jogs and superjogs and subsequent unzipping (see the text). $T = 400$ K and $\sigma_{\text{app}} = 50$ MPa. The length of dislocation shown is the total simulation length $L = 1000b = 0.245$ μm.

primary plane, we observe a lower probability for collision of kinks nucleated in different slip planes in that case.

The results presented in this section are obtained for non symmetrical triple slip conditions in which the MRSS plane bisects the primary glide plane at an angle of 15°. Our simulations indicate that the mobility of screw dislocations induced by this orientation of the MRSS plane approximately corresponds to the average dislocation mobility resulting from different shear stress orientations. The kink-pair nucleation rates in the different $\{\bar{1}10\}$ glide planes only depends on the magnitude and the direction of the MRSS—some possible non-Schmid effects (slip in the twinning direction is easier than the antitwinning direction [22]) are ignored thereby.

The time step Δt in the kMC model is the time that the system resides in the current state before the next transition. Δt depends on the total transition rate R and is randomly selected from the exponential distribution $f(t) = \mathrm{R}\,\mathrm{e}^{-R\Delta t}$. Since the total transition rate varies significantly with variations of the stress, temperature and hydrogen concentration, the difference between the time steps at different conditions differ by several orders of magnitude (see Table I and compare, for example, Figs. 9 and 10). The total times for which we study the migration of dislocations at different conditions are very different because we describe the evolution of a dislocation line as a result of approximately equal number of events generating statistical trajectories in the space of states. In our simulations, we determine the evolution of the average velocity of the dislocation. We evaluate the hydrogen effect on the dislocation mobility by comparing its average velocity with the average velocity of the dislocation in pure α-Fe, given in Table I.

B. Observed microstructure

Results from our simulations show that the behavior of the screw dislocation depends significantly on the applied shear stress, temperature, and hydrogen concentration in the bulk. At low applied shear stresses (≈50 MPa), hydrogen trapped in the dislocation core leads to the formation of pinning points and gradual immobilisation of screw dislocations. At 400 K, formation of pinning points occurs even in pure α-Fe as shown in Figs. 1 and 2. (This is an effect of the high temperature—at 300 K in pure α-Fe the dislocation advances without trailing any debris because kink formation is rare while kink migration is fast and so kinks seldom collide.) At 150 K, pinning begins at very low hydrogen concentrations of 0.001 appm, while at 300 K formation of jogs begins at 0.5 appm as shown in Figs. 3 and 4. Larger amounts of debris are produced at the same temperature and stress but higher hydrogen content. Pinning is initiated by the collision of two kinks nucleated in primary and cross slip planes and transformed into jogs by double cross slip. Because they cannot recombine and are constrained to move together, the kinks slow down or halt their coupled motion altogether. Such elementary jogs grow in size when more kinks pile up on either sides of the initial pinning point forming superjogs. The kinks in the pile-ups on two sides of the pinning point belong to different primary glide planes. If the dislocation lines on both sides of the pinning point cross each other they may reconnect by recombination of kink pairs. As a result, the dislocation line is now reduced in length, leaving behind a prismatic loop as shown for example in red as debris in Fig. 2. The cusps are easily released by this unzipping mechanism and straight dislocations along the screw direction are restored. The high unzipping rate leads to increased formation of debris behind the dislocation.

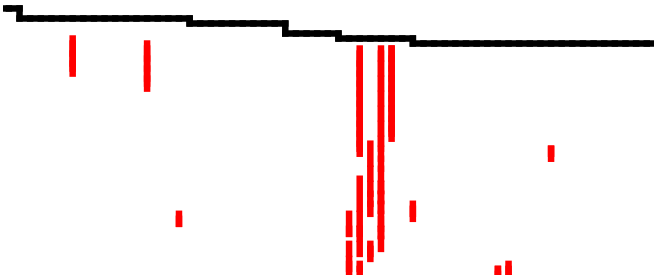

FIG. 2. A magnified section inside the boxed region of Fig. 1.

At low stress, the small probability for nucleation of kink pairs in secondary glide planes leads to lower probability for collision of two kinks propagating simultaneously in primary and cross slip planes. The probability of formation of kinks in both primary and cross slip planes increases with increasing temperature, which leads to increased probability for collision of kinks and pinning at 400 K. The rate of pinning is relatively low when the concentration of hydrogen atoms at the dislocation core binding sites is small. With increasing hydrogen concentration, the probability for nucleation of kink pairs in different glide planes increases, while the average kink velocity decreases due to the hydrogen trapping effect. The results from simulations confirm that the rate of pinning increases in this case while the unzipping rate decreases as seen in Figs. 3 and 4. The lower unzipping rate leads to accumulation of kinks and formation of superjogs (edge dipoles).

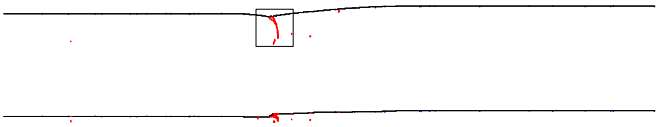

FIG. 3. Snapshot of a moving $\frac{1}{2}[111]$ screw dislocation (black line) projected onto $(\bar{1}10)$ and $(11\bar{2})$ planes as upper and lower lines, respectively. The red lines indicate debris left behind due to the creation of jogs and superjogs and subsequent unzipping (see the text). Blue dots represent the positions of hydrogen atoms. $T = 300$ K, $\sigma_{\text{app}} = 50$ MPa, and $C_{\text{H}} = 0.5$ appm. The length of dislocation shown is the total simulation length $L = 1000b = 0.245$ μm.

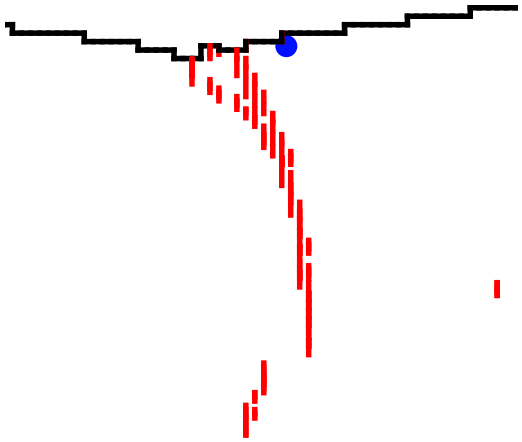

FIG. 4. A magnified section inside the boxed region of Fig. 3.

At higher stress (200 MPa) pinning at 150, 300, and 400 K starts, respectively, at hydrogen bulk concentrations of 0.001, 1, and 0 appm (as Fig. 1). Due to the high hydrogen concentration in the dislocation core at low temperatures, the hydrogen trapping effect leads to a reduction of the average kink velocity and increasing probability for the collision of kinks propagating simultaneously in different planes. This is illustrated in Figs. 5 and 6, which now show significant deviation from a straight dislocation on the primary slip plane and longer segments of trailing debris in the microstructure. At the same stress and higher temperature, the hydrogen trapping effect becomes smaller. In this case, the high probability for collision of kinks migrating simultaneously in different glide planes is mainly due to the increased probability for nucleation of kink pairs both in primary and the cross slip planes. This circumstance is illustrated in Figs. 7 and 8. It is interesting to observe that the number of hydrogen atoms decorating the dislocation in Fig. 7 is evidently fewer than in Fig. 5 even though the bulk hydrogen concentration is higher. This is because of the different temperatures used in the two simulations. At 400 K, although the bulk concentration is higher, the occupation probability of the traps is smaller, see Eq. (5). This is why the effects of hydrogen on dislocation mobility are limited above a certain high temperature at which hydrogen is effectively "boiled off" the dislocations [18].

C. Connection to HESIV

We would like to point briefly to the connection of our results to the *hydrogen-enhanced stress-induced vacancy*

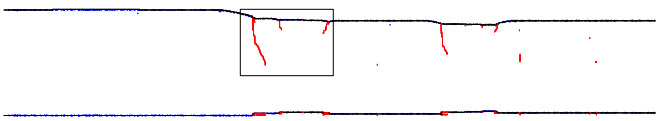

FIG. 5. Snapshot of a moving $\frac{1}{2}[111]$ screw dislocation (black line) projected onto $(\bar{1}10)$ and $(11\bar{2})$ planes as upper and lower lines, respectively. The red lines indicate debris left behind due to the creation of jogs and superjogs and subsequent unzipping (see the text). Blue dots represent the positions of hydrogen atoms. $T = 300$ K, $\sigma_{app} = 200$ MPa, and $C_H = 10$ appm. The length of dislocation shown is the total simulation length $L = 1000b = 0.245$ μm.

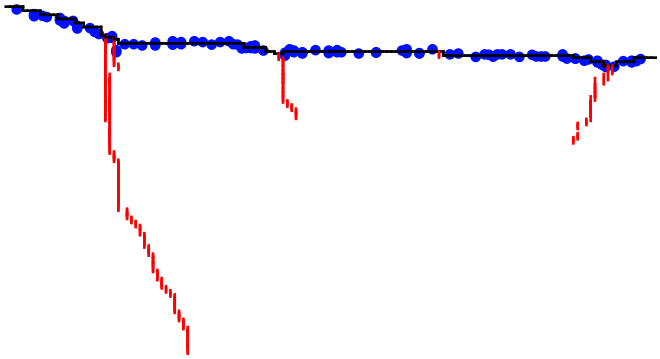

FIG. 6. A magnified section inside the boxed region of Fig. 5.

(HESIV) mechanism of hydrogen embrittlement [3]. This arises from some remarkable observations that put into question the role of the hydrogen atoms themselves in the reduction in toughness of iron. Takai *et al.* [29] made tensile stress–strain tests in pure Fe–3 wt%Si before and after charging with hydrogen. The expected reduction in strength and ductility was observed in the hydrogen charged specimens. However, if the hydrogen charged specimen was unloaded in middle of the test and the hydrogen outgassed, then on resuming the test the stress-strain behavior was the same *as in the hydrogen charged case.* This implies that the actual presence of hydrogen is not necessary in order to produce hydrogen embrittlement, but only that the hydrogen has an effect on the microstructure during deformation. This provides strong evidence for the hydrogen-induced "super abundance of vacancies" [30]. While it is hard to see how vacancies may be formed *ab initio* in a perfect lattice [31], it is most plausible that vacancies that are produced by the climb of jogs and the trailing of debris that we predict here are stabilized by the presence of hydrogen; and the microstructures that we find here which are attributed to dissolved hydrogen are the cause of the loss of ductility observed by Takai *et al.* [29].

D. Time evolution of dislocation velocity

Collision of kinks and the formation of pinning points leads to a gradual reduction of the average speed of the screw dislocation in hydrogen charged iron. These findings are illustrated in Figs. 9 and 10. At high hydrogen concentrations,

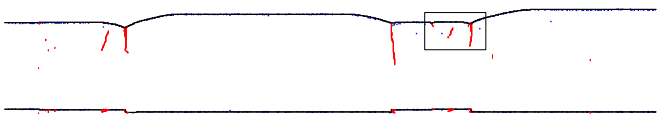

FIG. 7. Snapshot of a moving $\frac{1}{2}[111]$ screw dislocation (black line) projected onto $(\bar{1}10)$ and $(11\bar{2})$ planes as upper and lower lines, respectively. The red lines indicate debris left behind due to the creation of jogs and superjogs and subsequent unzipping (see the text). Blue dots represent the positions of hydrogen atoms. $T = 400$ K, $\sigma_{app} = 200$ MPa, and $C_H = 50$ appm. The length of dislocation shown is the total simulation length $L = 1000b = 0.245$ μm. Note that there are evidently fewer hydrogen atoms trapped per unit length of dislocation than in Fig. 5 although C_H is larger; this is because at higher temperature the trapping probability is reduced in accord with the McLean isotherm (5).

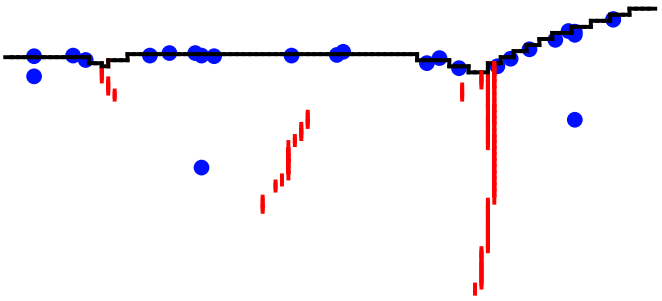

FIG. 8. A magnified section inside the boxed region of Fig. 7.

the hydrogen trapping effect and pinning lead to a reduction in the dislocation velocity to *below the speed of dislocations in pure iron*. In this way, we can observe both hydrogen hardening and softening and Figs. 9 and 10 allow us to explore the regimes of temperature, stress and hydrogen concentration at which each may be expected to be predicted [18]. For example, Figs. 9–11 show hardening at 300 K and 20 appm.

Remarkably, we do not observe pinning and immobilisation of screw dislocation at an applied shear stress of 100 MPa for any of the temperatures and hydrogen concentrations under consideration. The interplay between the hydrogen concentration, kink-pair nucleation rate and the kink migration velocity at $\sigma_{app} = 100$ MPa always leads to nucleation and propagation of only one kink pair along the entire dislocation line. Therefore the motion of screw dislocations at this stress is not impeded by the formation of jogs and debris and we observe the highest increase in dislocation velocity induced by hydrogen in α-Fe at low C_H. This situation can be seen from Fig. 11, showing a tenfold increase in dislocation velocity at 300 K, $\sigma_{app} = 100$ MPa, and $C_H = 1$, 3, and 10 appm, However, at $C_H = 20$ appm, the dislocation velocity is a factor of two smaller due to hydrogen (Fig. 11); however, our simulations show that this is not due to self-pinning as it is at $\sigma_{app} = 200$ (see Fig. 5) but is caused by solute hardening.

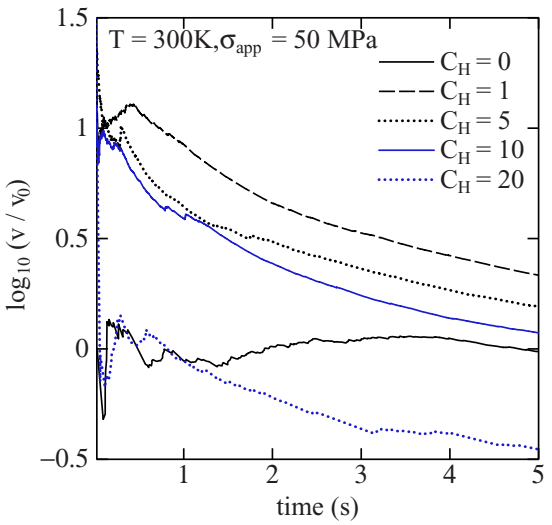

FIG. 9. The evolution of dislocation velocity with simulation time at various levels of bulk hydrogen concentration C_H, given in atomic parts per million. The velocity is indicated as the logarithm of the ratio of the actual velocity to that in pure iron at the same temperature and applied stress (see Table I). $T = 300$ K and $\sigma_{app} = 50$ MPa.

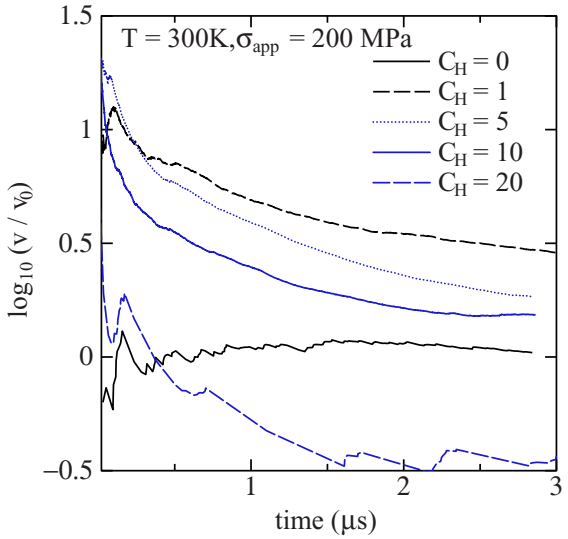

FIG. 10. The evolution of dislocation velocity with simulation time at various levels of bulk hydrogen concentration C_H, given in atomic parts per million. The velocity is indicated as the logarithm of the ratio of the actual velocity to that in pure iron at the same temperature and applied stress (see Table I). $T = 300$ K and $\sigma_{app} = 200$ MPa.

E. Effects of T, σ_{app}, and C_H on steady-state dislocation velocity

The effect of hydrogen on dislocation velocity is strongest at low temperature and low hydrogen concentration. At 150 K, the average velocity at $C_H = 0.0001$ appm is three orders of magnitude higher then the velocity in pure α-Fe as seen in Fig. 12. However, decreases in dislocation velocity and macroscopic hardening may be expected in the low temperature range with increasing hydrogen concentration above 0.001 appm due to the drag force generated by the

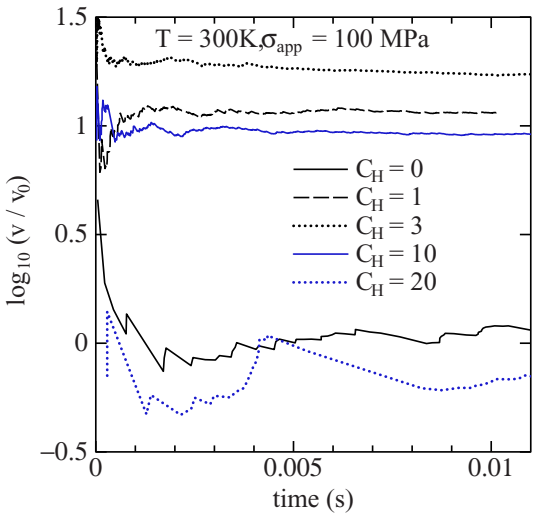

FIG. 11. The evolution of dislocation velocity with simulation time at various levels of bulk hydrogen concentration C_H, given in atomic parts per million. The velocity is indicated as the logarithm of the ratio of the actual velocity to that in pure iron at the same temperature and applied stress (see Table I). $T = 300$ K and $\sigma_{app} = 100$ MPa.

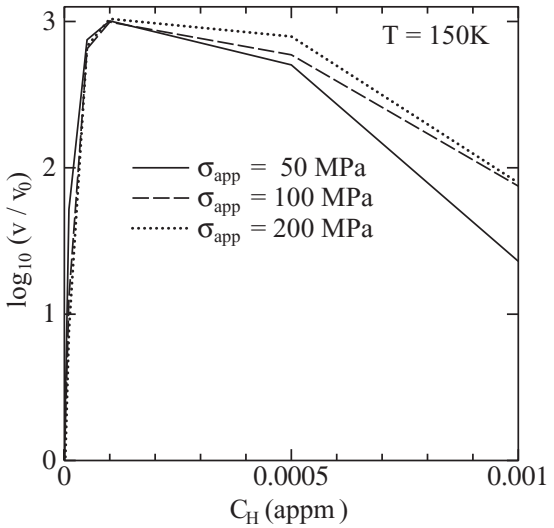

FIG. 12. Steady-state dislocation velocity as a function of bulk hydrogen concentration at 150 K and at the three applied stresses used in the present work. The velocity is indicated as the logarithm of the ratio of the actual velocity to that in pure iron at the same temperature and applied stress (see Table I). Note the one thousandfold increase in dislocation velocities at almost vanishingly small bulk hydrogen concentration. This is principally due the large amount of trapped hydrogen present at low temperature.

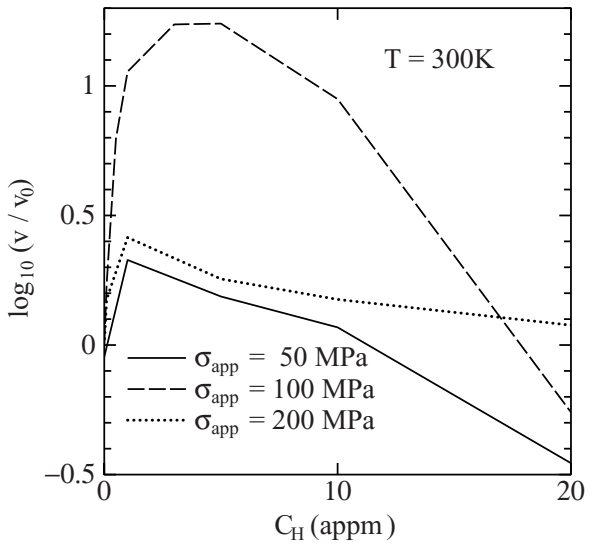

FIG. 13. Steady-state dislocation velocity as a function of bulk hydrogen concentration at 300 K and at the three applied stresses used in the present work. The velocity is indicated as the logarithm of ratio of the actual velocity to that in pure iron at the same temperature and applied stress (see Table I).

hydrogen atmospheres. Although hydrogen in α-Fe *increases* dislocation mobility at 150 K up to three orders of magnitude, the dislocation velocity is still 4–6 orders of magnitude *lower* than the velocity of a screw dislocation in pure α-Fe at 300 K. This reflects the well known very strong temperature dependence of dislocation velocity in bcc transition metals, see Table I.

The dependence of dislocation velocity on bulk hydrogen concentration at three applied stresses are shown at 150, 300, and 400 K in Figs. 12–14, respectively. We find that both decreases and increases of dislocation velocities due to hydrogen atmospheres are evident in the temperature interval 150–400 K. At $\sigma_{app} = 100$ MPa, the interval of hydrogen concentrations in which dislocation velocity increases most significantly widens with increasing temperature. In this way, at 150 K, the largest increase of dislocation mobility is observed in our simulations in the interval $C_H =$ 0–0.001 appm; at 300 K in the interval $C_H = 1$–10 appm and at 400 K in the interval $C_H = 5$–150 appm. At 300 K, the average velocity at $C_H = 3$ appm is more than an order of magnitude higher (see Fig. 13), while at 400 K and $C_H = 25$ appm it is 6–7 times higher than the velocity in pure bcc iron (Fig. 14). A decrease in dislocation mobility and hence macroscopic hardening may be expected at higher hydrogen concentrations as the hydrogen atmospheres generate a drag force and increase the probability for pinning of dislocation lines.

The initiation of shear localisation is a critical event that could be triggered either by external, geometrical or internal microstructural factors. Possible microstructural initiation sites are regions that undergo localized softening by some mechanism. The results of our kMC simulations indicate that an inhomogeneous distribution of hydrogen in the structure leads to formation of areas with enhanced or reduced dislocation velocity. The local increase of dislocation velocity leads to localized softening which can initiate shear localization. In the low-temperature range, dislocation velocity increases only in an extremely narrow interval of hydrogen concentration (Fig. 12). Although the velocity gradient with respect to hydrogen concentration in this case is very high, the probability for formation of hydrogen atmospheres in the interval $C_H = 0.00005$–0.0005 appm leading to significantly enhanced dislocation mobility is low. The interval of hydrogen

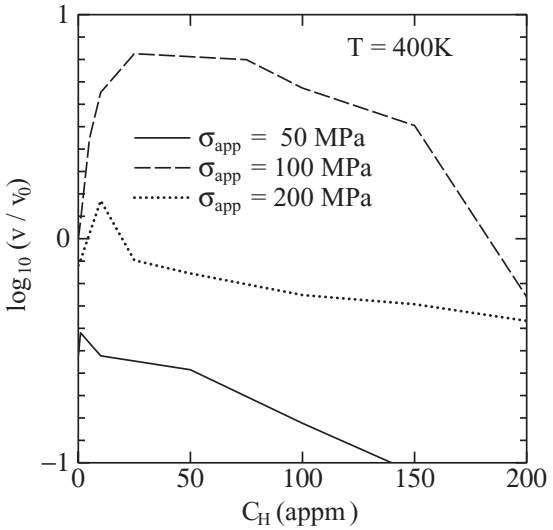

FIG. 14. Steady-state dislocation velocity as a function of bulk hydrogen concentration at 400 K and at the three applied stresses used in the present work. The velocity is indicated as the logarithm of ratio of the actual velocity to that in pure iron at the same temperature and applied stress (see Table I).

concentration in which dislocation velocity increases widens with increasing temperature, while the velocity gradient decreases (Figs. 12–14). With increasing concentration hydrogen trapping leads to lower dislocation velocity compared to the dislocation velocity in pure iron. Dislocation mobility predicted by our kMC simulations indicate that there exists an interval of optimal temperature and stress (about 100 MPa at 300 K) in which the inhomogeneous distribution of hydrogen may enhace significantly the probability for localized softening and hence the possibility of initiation of slip localisation.

IV. CONCLUSIONS

Our simulations show significant variation in the behavior of the $\frac{1}{2}[111]$ screw dislocation in α-Fe and we are able to identify the regimes of the applied shear stress, temperature and hydrogen concentration in bulk within which the dislocation velocity is either greater than or less than that in the absence of hydrogen. Moreover, by the use of a kMC model informed by DFT data on dislocation-hydrogen interactions, parameterized into a line tension model [18], we are able to make quantitative estimates of this velocity ratio. This exposes several key findings which will provide new microscopic understanding of the role of plasticity in hydrogen embrittlement.

(1) At low stress and low hydrogen content, the mobility of screw dislocations increases with bulk hydrogen concentration as a result of (i) increased kink-pair nucleation rate, (ii) low hydrogen trapping effect, and (iii) low probability for the formation of pinning points. With further increase in hydrogen content dislocation mobility decreases due to enhanced trapping effects and pinning by the formation of jogs and superjogs.

(2) At high stress and high temperature, the hydrogen trapping effect becomes less effective, and enhanced pinning and reduction of dislocation mobility occurs mainly due to the increased probability for nucleation of kink pairs both in the primary and cross slip planes.

(3) At high hydrogen concentration, the hydrogen trapping effect and pinning lead to a reduction of the dislocation velocity to below the speed of dislocations in pure iron at the same stress and temperature. This is the regime of hydrogen hardening [18].

(4) The interplay between kink-pair nucleation rate and the kink migration velocity at an applied resolved shear stress of 100 MPa leads to propagation of only one kink pair along the entire dislocation line. Therefore the motion of screw dislocations at this stress is not impeded by formation of jogs and debris and the kMC model predicts the highest increase in dislocation velocity induced by hydrogen in α-Fe.

(5) The effect of hydrogen on increasing dislocation velocity is strongest at low temperature and low hydrogen concentration.

(6) The range of hydrogen concentration within which dislocation velocity increases most significantly widens with increasing temperature.

(7) At room temperature, localized softening and thereby possible initiation of shear localisation could be expected under an applied stress close to 100 MPa and relatively low hydrogen content (viz. 1–10 appm).

(8) Screw dislocations can generate jogs and debris (prismatic loops) during their movement as a result of the collision and recombination of kinks. Both jogs and prismatic loops consist of edge dipoles, which are potential sources for multiplication and generation of new dislocations. The hydrogen trapped in the jogs and debris screens the elastic attraction between the edge dipoles. Hence an increase in the hydrogen concentration can reduce the barrier for activation of dislocation sources created as a result of screw dislocation movement. Furthermore, it is expected that by the defactant effect, vacancies created by the climb of jobs and by the expansion of prismatic loops will be stabilized by absorbing hydrogen thus enabling these processes at lower stress and temperature than in pure iron. The incorporation of this effect into our kMC simulations will be the subject of future work.

In conclusion, we have used published first-principles, quantum-mechanical (DFT) data on hydrogen dislocation interactions [18] to build a kinetic Monte Carlo model for the calculation of dislocation velocity in α-Fe as a function of stress, temperature, and bulk hydrogen concentration. Our results will provide a quantitative analysis of the HELP mechanism that was hitherto unavailable. Moreover, the dislocation velocities presented here will provide a breakthrough in the parametrization of discrete dislocation dynamics (DDD) simulations. At the same time the kMC described here and applied to just one dislocation at a time appears as a clear competitor to the DDD method if simulations are done involving a large number of dislocations admitting a greatly more realistic, physics-based description of plasticity. Additional electronic structure calculations will be needed to account for possible non-Schmid effects, dislocation-dislocation interactions, and to include carbon and substitutional alloying elements. This will be the subject of future work.

ACKNOWLEDGMENTS

We thank the anonymous referees for suggestions leading to significant improvement to the paper. We acknowledge the support of EPSRC under the Programme Grant HEmS, EP/L014742. Data supporting this research may be obtained by enquiry to research.data@kcl.ac.uk.

[1] I. H. Katzarov and A. T. Paxton, Phys. Rev. Materials **1**, 033603 (2017).
[2] A. T. Paxton, A. P. Sutton, and M. W. Finnis, Phil. Trans. R. Soc. A **375**, 20170198 (2017).
[3] M. Nagumo, *Fundamentals of Hydrogen Embrittlement* (Springer Nature, Singapore, 2016).
[4] C. D. Beachem, Metall. Trans. **3**, 441 (1972).
[5] S. P. Lynch, J. Mater. Sci. **21**, 692 (1986).
[6] S. P. Lynch, Acta Metall. **36**, 2639 (1988).
[7] D. Shih, I. Robertson, and H. Birnbaum, Acta Metall. **36**, 111 (1988).
[8] I. Robertson and H. Birnbaum, Acta Metall. **34**, 353 (1986).
[9] H. Birnbaum and P. Sofronis, Mater. Sci. Eng. A **176**, 191 (1994).

[10] J. Song and W. A. Curtin, Nat. Mater. **12**, 145 (2013).
[11] L. Ventelon and F. Willaime, J. Comput,-Aided Mater. Des. **14**, 85 (2007).
[12] C. R. Weinberger, G. J. Tucker, and S. M. Foiles, Phys. Rev. B **87**, 054114 (2013).
[13] R. Kirchheim, Acta Mater. **55**, 5129 (2007).
[14] R. Kirchheim, Acta Mater. **55**, 5139 (2007).
[15] R. Kirchheim, Scr. Mater. **62**, 67 (2010).
[16] R. Kirchheim, Scr. Mater. **67**, 767 (2012).
[17] M. Itakura, H. Kaburaki, and M. Yamaguchi, Acta Mater. **60**, 3698 (2012).
[18] M. Itakura, H. Kaburaki, M. Yamaguchi, and T. Okita, Acta Mater. **61**, 6857 (2013).
[19] V. V. Bulatov and W. Cai, *Computer Simulations of Dislocations*, 1st ed. (Oxford University Press, Oxford, 2006).
[20] W. Cai, V. V. Bulatov, S. Yip, and A. S. Argon, Mater. Sci. Eng. A **309-310**, 270 (2001).
[21] I. H. Katzarov and A. T. Paxton, Acta Mater. **59**, 1281 (2011).
[22] W. Spitzig, Acta Metall. **18**, 1275 (1970).
[23] H. Kimura and H. Matsui, Scr. Metall. **21**, 319 (1987).
[24] J. P. Hirth and J. Lothe, *Theory of Dislocations*, 1st ed. (McGraw-Hil Book Company, New York, 1968).
[25] D. Caillard, Acta Mater. **58**, 3493 (2010).
[26] I. H. Katzarov and A. T. Paxton (unpublished).
[27] A. Y. Kuksin and A. V. Yanilkin, Phys. Solid State **55**, 1010 (2013).
[28] C. Deo, D. Srolovitz, W. Cai, and V. Bulatov, J. Mech. Phys. Solids **53**, 1223 (2005).
[29] K. Takai, H. Shoda, H. Suzuki, and M. Nagumo, Acta Mater. **56**, 5158 (2008).
[30] Y. Fukai, *The Metal–Hydrogen System*, 2nd ed. (Springer-Verlag, Berlin Heidelberg, 2005).
[31] F. F. Dear and G. C. G. Skinner, Philos. Trans. R. Soc. A **375**, 20170032 (2017).